Giant coercivity and spin clusters in high pressure polymorphs of Mn2LiReO6

Giant coercivity and spin clusters in high pressure polymorphs of Mn_2LiReO_6.

Received 00th January 20xx,
Accepted 00th January 20xx

DOI: 10.1039/x0xx00000x

Elena Solana-Madruga,*[abc] Clemens Ritter,[d] Olivier Mentré,[a] J. Paul Attfield[b] and Ángel M. Arévalo-López.*[a]

We present Mn_2LiReO_6 synthesised at high pressure in two different polymorphs. They are the only A-site manganites with an ideal +/7+ charge distribution over the B/B' sites. The lower pressure polymorph crystallises in a polar *R*3 ordered-ilmenite type structure (OIL) with a calculated 26.9 μC/cm^2 electrical polarisation. It shows a cluster spin glass behaviour due to Li/Mn anti-site mixing. The well-ordered higher-pressure double-perovskite polymorph (DPv, $P2_1/n$) develops weak-ferromagnetism with giant magnetic coercivity (H_C = 6.9 T at 2 K) due to magnetocrystalline anisotropy enhanced by symmetry-restricted exchange interactions but in absence of spin-orbit coupling.

Introduction

Magnetic materials with large coercivity are desirable as permanent magnets. [1] However, there is a need to move away from rare-earth-based hard-magnets. In oxides, besides the hexaferrites just a handful of materials show giant or even large magnetic coercivities and it is thus important to understand the mechanisms to obtain those values. Magnetic coercivity is often determined by magnetocrystalline anisotropy, mainly controlled by spin-orbit-coupling (SOC). For instance in $Sr_5Ru_{4.1}O_{15}$, weak ferromagnetism in combination with the non-zero orbital moment of Ru accounts for the giant coercivity of 12 T at 1.7 K. [2] In the double perovskites (DPv) La_2CuIrO_6, [3] $La_2Ni_{1.19}Os_{0.81}O_6$ [4] and Lu_2NiIrO_6 [5] the combination of magnetocrystalline anisotropy along with frustration or defects were found to favor the large H_C values of 1.2 T (10 K), 4.1 T (5 K) and 4.8 T (5 K) respectively. Besides the significance of SOC present in the above materials, the pining of domain walls also plays a crucial role for coercivity enhancement. For instance, in single crystals of $LuFe_2O_4$ giant coercivity values of 9 T and 11 T at 4 K were reported. [6, 7] The orbital magnetic moment of Fe^{2+}, as a source of uniaxial magnetocrystalline anisotropy and the collective freezing of ferrimagnetic bidimensional domains are responsible for such values. It is thus imperative to establish if SOC is a requirement or not in order to observe giant coercivities in oxides. As an obvious strategy, the observation of huge coercivities in compounds without SOC would shed some light on the different required ingredients.

In this work, we have introduced the small Mn^{2+} ($3d^5$, S = 5/2, L = 0) into the A-site of A_2LiReO_6 by high-pressure and high-temperature synthesis. Two new Mn_2LiReO_6 polymorphs with ordered-ilmenite (OIL) and DPv-type structures were discovered. Both compounds show a charge distribution +/7+ among the *B/B'* sites and complex magnetic behaviours. The OIL presents an example of cluster spin glass behaviour below 46 K. The DPv shows a hard - weak ferromagnetic (WFM) behaviour without SOC below 109 K and with a giant magnetic coercivity of 6.9 T at 2K. These results motivate the search for hard magnetic materials without SOC cations and clarifies the role of cation order/disorder effects on obtaining giant coercivities.

Results and discussion

Mn_2LiReO_6 oxides were prepared under high pressure (5 GPa – OIL and 8 GPa – DPv) and high temperature (1100 ˚C) conditions using a Walker-type multianvil press. Further experimental details can be found in the Supporting Information. Figure 1 shows the Rietveld fits (a) and a comparative projection of the structural models (b) for the Mn_2LiReO_6 OIL and DPv polymorphs refined against 300 K neutron powder diffraction (NPD) D20 data. Structural details of the refined structures are summarised in Tables 1 and 2 respectively.

The lower-pressure polymorph crystallises with an OIL-type structure in the *R*3 polar space group with cell parameters a = 5.2515(3) Å and c = 13.8444(9) Å. Alternating *ab* honeycomb layers stacked along the *c* direction consist of perfectly ordered Mn1/Re and disordered Mn2/Li2 (0.56/0.44) edge shared octahedra. The main distortion in OIL_Mn_2LiReO_6 and corundum-based structures is the puckering of the honeycomb layers, induced by the cation shifts along the *c* axis due to

[a] *UMR-8181-UCCS- Unité de Catalyse et Chimie du Solide -Univ. Lille, CNRS, Centrale Lille, ENSCL, Univ. Artois, F-59000 Lille, France. E-mail: *angel.arevalo-lopez@univ-lille.fr, elsolana@ucm.es*

[b] *Centre for Science at Extreme Conditions (CSEC) and School of Chemistry. The University of Edinburgh, EH9 3FD, U.K.*

[c] *Departamento de Química Inorgánica, Facultad CC. Químicas, Universidad Complutense de Madrid, Spain.*

[d] *Institut Laue-Langevin, 71 Avenue des Martyrs, 32042, Grenoble Cedex, France.*

Electronic Supplementary Information (ESI) available: [details of any supplementary information available should be included here]. See DOI: 10.1039/x0xx00000x

Coulomb interactions between cations in face-shared octahedra. The large charge difference between (Mn1/Re) and (Mn2/Li) layers results in a strong cooperative off-centring and induce a notable spontaneous polarisation, estimated to be 26.9 μC/cm^2 via point charge model calculation. Nominal oxidation states for Mn^{2+}, Li^+ and Re^{7+} are confirmed from BVS calculations, where mixed occupations for Mn and Li are considered for the disordered layer. Constraints for the atomic displacement parameters were necessary. A small amount of $LiMn_2O_4$ (4.6 wt%) secondary phase was observed from NPD data.

Table 1. Atomic positions and main interatomic distances of OIL_Mn_2LiReO_6 as refined from the 300K D20 NPD data. Space group *R3* and cell parameters a = 5.2515(3) Å and c = 13.8444(9) Å. Agreement factors: R_p = 1.30%, R_{wp} = 1.81 %, R_B = 6.23%, R_f = 5.39%, χ^2 = 5.19%.

Site	x	y	z	Occ	B_{iso} (Å^2)
Mn1 (3a)	0.0	0.0	0.035(1)	1	1.1(1)
Mn2 (3a)	0.0	0.0	0.539(1)	0.562(7)	1.1(1)
/ Li2				0.438(7)	
Li1 (3a)	0.0	0.0	0.832(5)	0.562(7)	1.1(1)
/ Mn3				0.438(7)	
Re (3a)	0.0	0.0	0.328(1)	1	1.1(1)
O1 (9b)	0.310(2)	0.030(4)	0.25 [a]	1	1.57(7)
O2 (9b)	0.694(4)	0.048(4)	0.7426(4)	1	1.57(7)

Bond A-O	Length (Å)	Bond B'-O	Length (Å)
(Mn1-O1)x3	2.40(1)	(Re-O3)x3	1.90(1)
(Mn1-O2)x3	2.03(1)	(Re-O2)x3	1.93(3)
$\Delta[MnO_6]*10^5$	698	$\Delta[ReO_6]*10^5$	6.14
[b]d_{Mn1} (Å)	0.538	[b]d_{Re} (Å)	-0.015
Bond A'-O	Length (Å)	Bond B-O	Length (Å)
(Mn2-O1)x3	2.07(3)	(Li1-O1)x2	2.11(5)
(Mn2-O2)x3	2.39(3)	(Li1-O2)x2	2.14(6)
$\Delta[Mn2O_6]*10^5$	515	$\Delta[Li1O_6]*10^5$	4.98
[b]d_{Mn2} (Å)	0.636	[b]d_{Li} (Å)	0.033
BVS_{Mn1}	BVS_{Mn2}	BVS_{Li1}	BVS_{Re}
2.16	2.05	0.82	7.02

[a] O1 z position used as a cell reference. [b] d_i stands for the cation shift along c from the octahedral centre.

Table 2. Atomic positions and main interatomic distances and angles of DPv_Mn_2LiReO_6 as refined from the 300 K D20 NPD data. Space group $P2_1/n$ and cell parameters a = 5.2396(5) Å, b = 5.3916(5) Å, c = 7.6480(7) Å and β = 89.92(1) °. Agreement factors: R_p = 7.58%, R_{wp} = 9.59 %, R_B = 6.48%, R_f = 3.60%, χ^2 = 0.96%.

Site	x	y	z	B_{iso} (Å^2)
Mn (4e)	0.508(2)	0.458(2)	0.250(1)	0.9(1)
Li (2d)	0.5	0.0	0.0	0.52(9)
Re (2c)	0.0	0.5	0.0	0.52(9)
O1 (4e)	0.120(1)	0.563(1)	0.241(1)	1.01(7)
O2 (4e)	0.686(1)	0.682(1)	0.059(1)	1.01(7)
O3 (4e)	0.830(1)	0.198(1)	0.068(1)	1.01(7)

Bond A-O	Length (Å)	Bond A-O	Length (Å)
Mn-O3	2.08(1)	Mn-O3	2.59(1)
Mn-O2	2.11(1)	Mn-O2	2.63(1)
Mn-O1	2.11(1)	Mn-O2	2.68(1)
Mn-O1	2.23(1)	Mn-O3	2.74(1)
Bond B-O	Length (Å)	Bond B'-O	Length (Å)
(Li-O1)x2	2.10(1)	(Re-O1)x2	1.98(1)
(Li-O2)x2	2.023(9)	(Re-O2)x2	1.97(1)
(Li-O3)x2	2.096(9)	(Re-O3)x2	1.930(9)
$\Delta[LiO_6]*10^4$	2.91	$\Delta[ReO_6]*10^4$	1.21
Li-O1-Re	139.0(4)º	Tilt	Angle
Li-O2-Re	140.8(6)º	Φ	20.5(2)º
Li-O3-Re	138.0(6)º	θ	20.3(3)º
	Mn	Li	Re
BVS	1.98	1.17	6.20

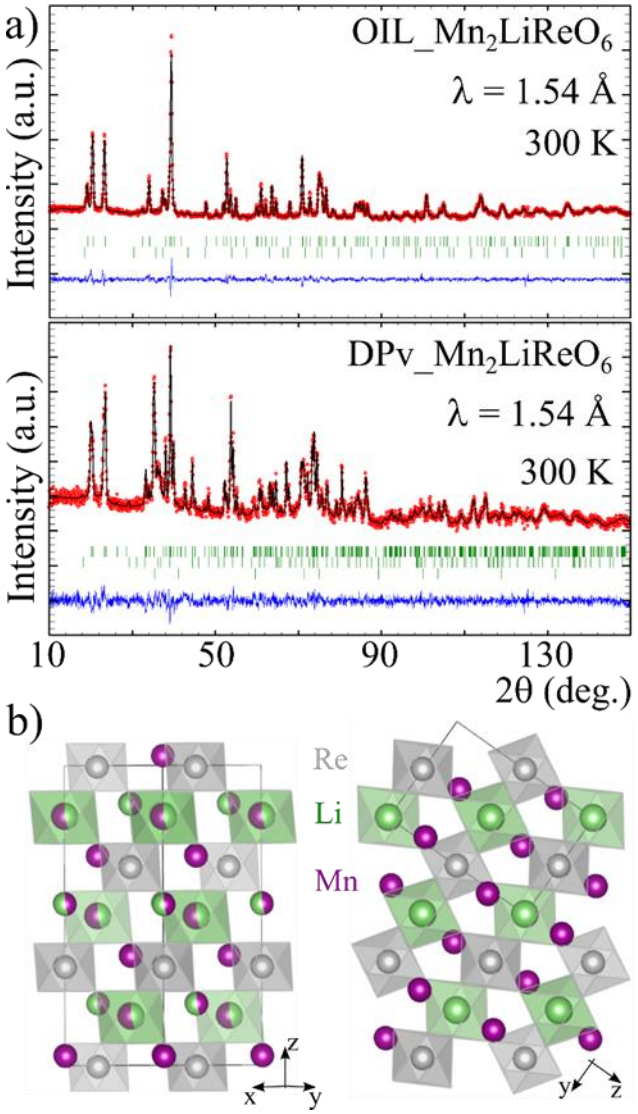

Figure 1. Rietveld fits (a) of the OIL (top) and DPv (bottom) polymorphs of Mn_2LiReO_6 from 300 K D20 NPD data. The secondary phases are $LiMn_2O_4$ (4.6 wt%) for OIL and Mn_3O_4 (20 wt%) and MnO (12 wt%) for the DPv. The respective refined structural models are comparatively shown in b).

The higher-pressure polymorph crystallises with a $P2_1/n$ DPv structure with a = 5.2396(5) Å, b = 5.3916(5) Å, c = 7.6480(7) Å and β = 89.92(1) ° cell parameters. Rietveld refinements confirm full occupancy without any antisite mixing, tested for both *B/B'* and *A/B* sites, in agreement with the large charge/size mismatches. Constraints for the atomic displacement parameters were necessary. Secondary phases of Mn_3O_4 (20 wt%) and MnO (12 wt%) were only observed in NPD data as a result of the metastability of the DPv_Mn_2LiReO_6.

The half-filled $3d^5$ electron configuration of Mn^{2+} and the full shells of Li^+ and Re^{7+} cations would imply an isotropic distribution of the valence orbitals and hence favours small polyhedral distortions. However, Mn^{2+} in the large *A* site void of the DPv structure reduces considerably the tolerance factor (t = 0.82) from the related cubic Ba_2LiReO_6 (t = 1.04) and Sr_2LiReO_6 (t = 0.98) and thus large octahedral tilts of φ = 20.5 ° and θ = 20.3 ° along the c axis and in the ab plane respectively are necessary. These are comparable to those observed in other

Mn_2BReO_6 (B = Fe, Mn, Co and Ni) high pressure double perovskites. [8-13]

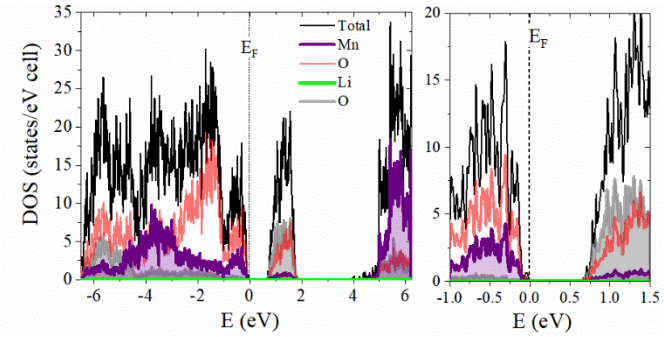

Figure 2. Calculated density of states for DPv_Mn_2LiReO_6.

Nominal Mn^{2+} and Li^{+} oxidation states are confirmed from estimated BVS values. However, rhenium shows a lower value than expected (6.2+, see Table 2), the likely reasons being the strain imposed on the oxygens in order to accommodate Mn^{2+} and the more covalent character of the Re-O bonds when compared to Li-O/Mn-O, in accordance with the higher-pressures required to obtain this polymorph. This is also confirmed by DFT calculations where nearly zero magnetic moment is observed for rhenium, in agreement with the Re^{7+} formal valence. The density of states (DOS) also shows a narrow band gap (0.65 eV) with the lowest part of the conduction band dominated by empty Re d and O p states, consistent with the dark colour of the sample (see Figure 2 and ESI for calculation details).

The bulk magnetic susceptibility of OIL_Mn_2LiReO_6 presents a transition at 46 K with a field cooled-zero field cooled (FC – ZFC) divergence, pointing towards a canted antiferromagnetic or spin-glass behaviour, see Figure 3a. Curie Weiss fit to the inverse susceptibility above 175 K results in θ = -196(1) K, supporting strong AFM interactions. The calculated effective magnetic moment of 5.87(3) μ_B / Mn^{2+} agrees well with the expected value of 5.92 μ_B for a d^5 cation (S = 5/2). It also shows a large frustration index of $f = |\theta|/T_N = 4.3$ among the $Mn_2BB'O_6$ ordered-corundum related structures (see Table S2). NPD data collected at 2 K showed only short-range order correlations without any coherent magnetic maxima (ESI Fig. S5). AC-magnetic susceptibility was subsequently measured on a fresh sample and revealed a spin-glass behaviour with a shift of the freezing temperature T_F of 1.6 K (Fig. 2b). The temperature evolution of T_F follows the Vogel- Fulcher equation $\omega = \omega_0 \exp[E_a/k_B (T_F-T_0)]$ with ln (ω_0 / Hz) = 18.8(1) (1/ $\omega_0 = \tau_0$ = 6.8 ·10^{-9} s), T_0 = 46.2(1) K and E_a/k_B = 45.3(1) K. These values strongly suggest the formation of a cluster spin glass ($\tau_0 \approx 10^{-7} - 10^{-10}$ s) below T_F, as recently observed in $CaMnFeTaO_6$.[15] The main reason of this behaviour is presumably the disorder between Mn and Li in one of the layers.

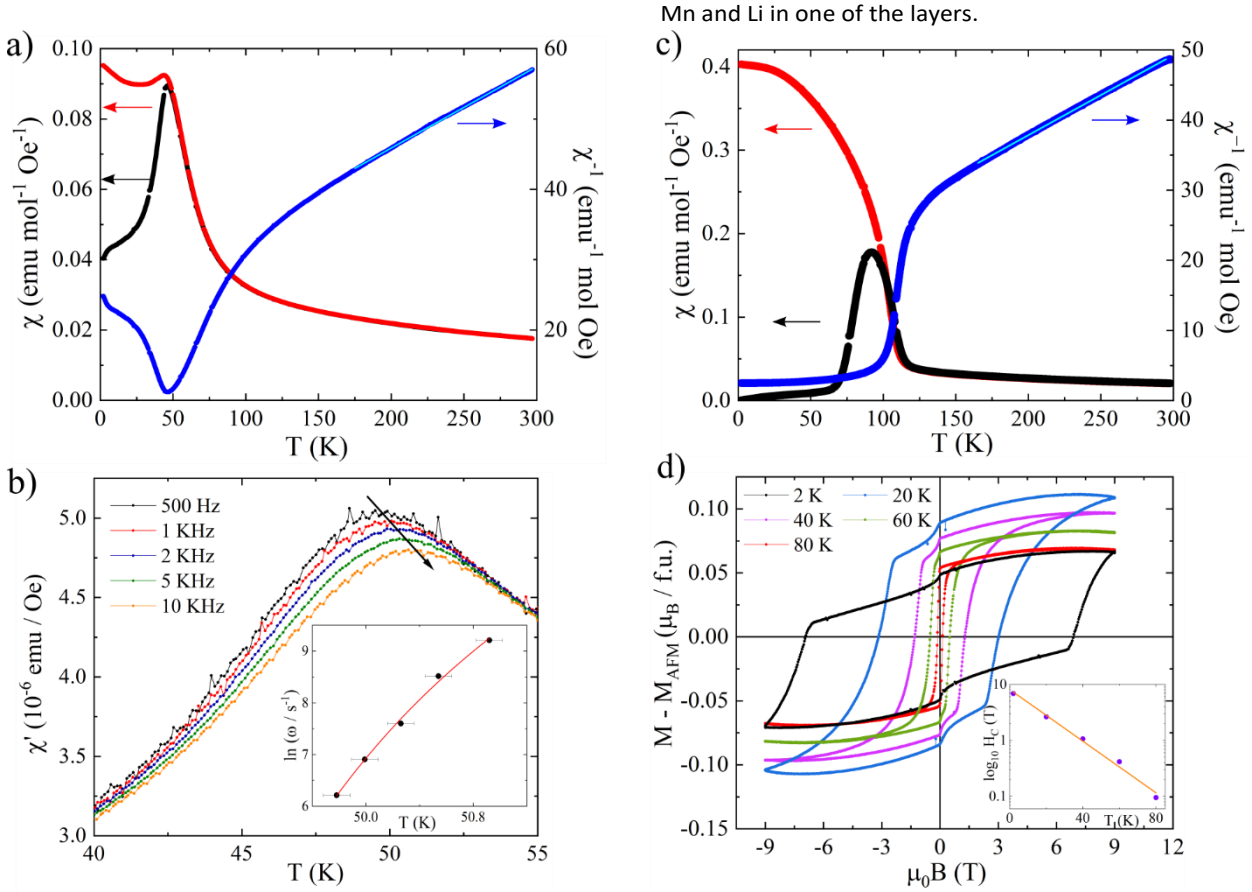

Figure 3. Magnetic properties of OIL(left) and DPv_Mn_2LiReO_6 (right). Bulk magnetic susceptibility of OIL (a) and DPv (c) polymorphs with ZFC-FC (black-red) and inverse susceptibility (blue) with CW fit above 175 K. b) AC magnetisation of OIL_Mn_2LiReO_6, showing frequency dependent freezing temperature T_F. Inset shows fit of the T_F evolution to the Vogel-Fulcher equation. d) Hysteresis loops of DPv_Mn_2LiReO_6 after AFM contribution subtracted, see text. Inset shows the fitted logarithmic dependence of H_C with temperature.

For the higher-pressure DPv_Mn_2LiReO_6, magnetic susceptibility measurements show a magnetic transition at T_N = 109 K with a strong FC – ZFC divergence at lower temperatures (Fig. 3c). The fit of the reciprocal susceptibility to the Curie-Weiss law above 175 K suggests strong AFM interactions with θ = -134(1) K. The calculated effective magnetic moment of 5.61(4) μ_B / Mn^{2+} is again in good agreement with the expected value of 5.9 μ_B. However, an unusual behaviour is observed in the field dependent magnetisation measurements below 100 K (see Fig. S2). At this temperature, a weak-ferromagnetic component of 0.03 μ_B is present, which becomes much harder but not much larger on cooling, with a maximum coercive field of H_C = 6.9 T at 2 K. To appreciate the extreme hardening behaviour of DPv_Mn_2LiReO_6, the hysteresis loops have been subtracted from the linear AFM $M(H)$ response (Fig. 3d). Small steps are appreciated in the low magnetic field region, which account for up to ~ 15 % of the total magnetisation M_0 at 2 K and are due to smoothly reoriented domains.

The temperature dependence of the coercive field H_C has been plotted in a semi-log plot scale in the inset of Figure 3d. Linear relations between $H_C \propto T$ and $H_C^{1/2} \propto T^{2/3}$ are predicted for so-called weak and strong domain wall pinning, respectively. [16]

However, DPv_$MnLiReO_6$ clearly shows an exponential strong hardening behaviour. The detailed mechanism of giant coercivity is not generally understood. Nevertheless, large magneto-crystalline anisotropy is partly responsible, for instance, in the WFM $Sr_5Ru_{5-x}O_{15}$ or the ferrimagnet $LuFe_2O_4$ with respective coercivities of 12 T and 9 T at low temperatures.[2,6]

Although large magnetocrystalline anisotropy is expected in DPv due to low-symmetry crystal structure and the presence of heavy atoms as in La_2CuIrO_6, $La_2Ni_{1.19}Os_{0.81}O_6$ and La_2NiIrO_6; [3-5] such large values are without precedent in DPv_Mn_2BReO_6 A-site manganites (B = Mn, Fe, Co, Ni). [8-13] This suggests that for DPv_Mn_2LiReO_6, the lack of d electrons for Li^+ ([He]) and Re^{7+} ([Xe]$4f^{14}$) add a further ingredient in the search for rare-earth-free hard magnets.

It is also notable that the maximum ferromagnetic moment at 20 K takes a relatively large value of 0.11 μ_B / f.u. but collapses to a 60% of its value (0.067 μ_B / f.u.) at 2 K (see Fig. 3d). Since the spins become more ordered on cooling below 20 K while the weak-ferromagnetic component decreases in magnitude, this implies a spin reorientation as observed for instance in Mn_2NiReO_6. [13] AC susceptibility measurements provide further evidence of this behaviour showing a plateau for χ'(T) in the 20 - 70 K temperature range, below which the magnetisation is reduced (see Fig. S4).

3 K NPD data reveal that DPv_Mn_2LiReO_6 orders into a collinear magnetic structure with propagation vector k = [0 0 0]. Mn spins are AFM coupled in ab layers with a refined moment of 2.4(1) μ_B/Mn. These layers are separated by non-magnetic B-B' Li^+-Re^{7+} octahedra and stacked FM along the c direction with the spins confined in the ac plane as shown in Figure 4b. The FM net component observed in magnetisation measurements is below the resolution limit of our data. Attempts to include it as a b component in the Mn spins as it is allowed by symmetry (see Table S1), resulted in unstable refinements. The broadening of the magnetic peaks also suggests a short magnetic coherence length estimated to ~ 1/5 of the crystalline coherence length from the Scherrer equation, which likely explains the low value of the refined magnetic moment. [17]

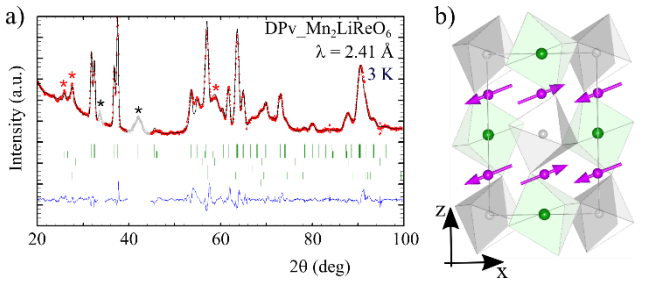

Figure 4. a) Rietveld fit of the 3 K NPD pattern and b) its refined magnetic structure. MnO and Mn_3O_4 are included as secondary phases. Red and black asterisks mark respectively magnetic reflections and excluded spurious signals from the diffractometer. Grey/ green octahedra represent Re/Li octahedra, Mn atoms are in purple.

In comparison with similar A-site manganites, DPv_Mn_2LiReO_6 presents exclusive factors that may explain the unprecedented giant coercivity values observed. The other four existent DPv_Mn_2BReO_6 (B = Mn^{2+}, Fe^{3+}, Co^{2+}, Ni^{2+}) [8-13] contain Re in either 5+ ($5d^2$) or 6+ ($5d^1$) oxidation states with not-quenched SOC. The absence of giant coercivities in these compounds discards a possible rhenium spin-orbit-coupling origin in A-site DPv manganites. Mn_2ScSbO_6 and Mn_2CoTeO_6 present similar magnetic structures for the Mn A-sublattice, but again, without the presence of giant coercivity. [18,19]

In DPv_Mn_2LiReO_6, the WFM component is forced by symmetry to lie along the unique b axis. This symmetry requirement along with the Mn distorted coordination induce enough magnetocrystalline anisotropy to observe giant coercivity.

The global magnetic behaviour of DPv_Mn_2LiReO_6 can therefore be understood in terms of small WFM domains. Increasing their sizes requires a high energy to rotate the domain walls (exponential pinning) due to magnetocrystalline anisotropy enhanced by the structural restrictions, and thus results in this uniquely hard A-site manganite without the requirement of spin-orbit coupling. The combination of structurally constrained exchange interactions with magnetocrystalline anisotropy appears to favour huge coercivities and may help in the search for rare-earth-free hard magnets.

Conclusions

In conclusion, two new A-site manganites Mn_2LiReO_6 with ordered ilmenite-type (OIL) and double perovskite (DPv) structures are presented. They are relevant as the first +/7+ based A-site manganites, suggesting accessibility to a new set of compounds and the chemical control of their physical properties. OIL_Mn_2LiReO_6 shows a large magnetic frustration inducing a spin-cluster behaviour unique among double corundum oxides. This is combined with the spontaneous polarisation of 26.9 $\mu C/cm^2$ in this $R3$ material. DPv_Mn_2LiReO_6 is a "hard-weak FM" with a giant coercive field of 6.9 T. The origin of this can be related to an enhanced magnetocrystalline

anisotropy via restricted exchange interactions along with small domain size and low crystal symmetry. This study also demonstrates the polymorphism in rhenates among *A*-site manganites, for which only DPv phases had been observed before. This suggests perovskite related phases could also be accessible at higher pressures for the corundum-related oxides $Mn_2BB'O_6$ with *B'* = Nb, Ta, Mo, W, setting the ground for new materials research.

Author Contributions

The study was designed by AMAL. Synthesis was performed by ESM and AMAL. Bulk magnetism data were measured and analysed by ESM and AMAL. Neutron diffraction data were collected and analysed by ESM, AMAL and CR. DFT calculations were done by OM. The paper was written by ESM and AMAL with collaborations from all authors.

Conflicts of interest

There are no conflicts to declare.

Acknowledgements

We thank support from ANR AMANTS project (19-CE08-0002-01) and the ILL for beamtime at D20. The Chevreul Institute (FR 2638), Region Hauts-de-France, and FEDER are acknowledged for funding the X-ray diffractometers, the “LEGO” multianvil-press and the PPMS magnetometer.

Notes and references

1 E. A. Gorbachev, E. S. Kozlyakova, L. A. Trusov, A. E. Sleptsova, M. A. Zykin, P. E. Kazin. *Russ. Chem. Rev.* 2021, **90** (10) 1287 – 1329.
2 W. Wu, V. Kiryukhin, H.-J. Noh, K.-T. Ko, J.-H. Park, W. Ratcliff II, P. A. Sharma, N. Harrison, Y. J. Choi, Y. Horibe, S. Lee, S. Park, H. T. Yi, C. L. Zhang, S.-W. Cheong. *Phys. Rev. Lett.* **101**, 137203.
3 J. Iida, M. Tanaka, Y. Nakagawa, S. Funahashi, N. Kimizuka, S. Takekawa. *J. Phys. Soc. Jpn.* 1993, **62**, 1723.
4 A. Yamamoto, D. Hashizume, H. A. Katori, T. Sasaki, E. Ohmichi, T. Nishizaki, N. Kobayashi, H. Takagi. *Chem. Mater.* 2010, **22**, 5712–5717.
5 X. Zhang, B. Li, J. Cheng, X. Chen, L. Wang, Z. Miu, Z. Song, F. Chi, S. Liu and Z. H. Wang. *J. Phys.: Condens. Matter* 2019, **31**, 435601.
6 H. L. Feng, M. Reehuis, P. Adler, Z. Hu, M. Nicklas, A. Hoser, S.-C. Weng, C. Felser, M. Jansen. *Phys. Rev. B* **97**, 184407.
7 P. C. Rout, U. Schwingenschlögl. *Nano Lett.* 2021, **21**, 16, 6807–6812.
8 M.-R. Li, M. Retuerto, Z. Deng, P. W. Stephens, M. Croft, Q. Huang, H. Wu, X. Deng, G. Kotliar, J. Sánchez-Benítez, J. Hadermann, D. Walker, M. Greenblatt. *Angew. Chem., Int. Ed.* 2015, **54**, 12069–12073.
9 A. M. Arévalo-López, G. M. McNally, J. P. Attfield. *Angew. Chem. Int. Ed.* 2015, **54**, 12074–12077.
10 M.-R. Li, J. P. Hodges, M. Retuerto, Z. Deng, P. W. Stephens, M. C. Croft, X. Deng, G. Kotliar, J. Sánchez-Benítez, D. Walker, M. Greenblatt. *Chem. Mater.* 2016, **28**, 3148–3158.
11 A. M. Arévalo-López, F. Stegemann, J. P. Attfield. *Chem. Commun.* 2016, **52**, 5558–5560.
12 C. E. Frank, E. E. McCabe, F. Orlandi, P. Manuel, X. Tan, Z. Deng, M. Croft, V. Cascos, T. Emge, H. L. Feng, S. Lapidus, C. Jin, M. X. Wu, M. R. Li, S. Ehrlich, S. Khalid, N. Quackenbush, S. Yu, D. Walker, M. Greenblatt. *Chem. Commun.*, 2019, **55**, 3331–3334.
13 E. Solana-Madruga, K. N. Alharbi, M. Herz, P. Manuel, J. Paul Attfield. *Chem. Commun.*, 2020, **56**, 12574.
14 T. Klimczuk, H. W. Zandbergen, Q. Huang, T. M. McQueen, F. Ronning, B. Kusz, J. D. Thompson, R. J. Cava. *J. Phys.: Condens. Matter* 2009, **21**, 105801.
15 P. Kearins, E. Solana-Madruga, K. Ji, C. Ritter, J. Paul Attfield. *J. Phys. Chem. C* 2021, **125**, 17, 9550–9555
16 P. Gaunt. *Canadian Journal of Physics*, 1987, 65, 1194.
17 A. Fajar, Gunawan, E. Kartini, H. Mugirahardjo, M. Ihsan. *Atom Indonesia*, 2010, **36**, 3, 111 – 115.
18 E. Solana-Madruga, A. J. Dos santos-García, A. M. Arévalo-López, D. Ávila-Brande, C. Ritter, J. P. Attfield, R. Sáez-Puche. *Dalton Trans.* 2015, **44**, 20441–20448.
19 E. Solana-Madruga, C. Ritter, C. Aguilar-Maldonado, O. Mentré, J. P. Attfield, Á. M. Arévalo-López. *Chem. Commun.* 2021, **57**, 8441–8444

Please do not adjust margins